COMPOSITE CERAMIC ARMOR DEFECT DETECTION ANALYSIS USING PHASED ARRAY ULTRASOUND

J. S. Steckenrider
Illinois College
Jacksonville, IL

T.J. Meitzler and Lisa Prokurat Franks
US Army, TARDEC
Warren, MI

W. A. Ellingson
Argonne National Laboratory
Argonne, Illinois USA

ABSTRACT

A series of 16-inch square by 2-inch thick, multi-layered ceramic composite armor specimens, some of which had intentional design defects inserted between the layers, were inspected using a 128 element, 10MHz immersion phased array ultrasound system. To overcome some of the issues associated with the acoustic wave propagation in layered media, two digital signal processing methods (Fast Fourier Transform (FFT) and Wiener filtering) were employed. While previous work has been presented on the significant improvement in defect detection associated with these methods, the authors present a detailed and quantitative statistical analysis of these results. This analysis suggests that these intentional defects were a) not detectable when the defect was in a particular configuration, b) readily detectable in all cases for alternate defect position configurations, and c) clearly identifiable in most cases for those configurations. However, even in the configuration where intentional defects were not detected (owing to inherent design issues in the armor structure), significant variation in interfacial quality was observed and quantified, and these results will also be presented.

INTRODUCTION

Although ceramic vehicular armor offers significant potential improvement over historical materials by providing a greater capacity for energy absorption and dissipation per unit mass (i.e., very high fracture toughness), they are more susceptible to manufacturing defects that may reduce that high toughness. Thus, an efficient non-destructive evaluation (NDE) method which can both identify and quantify these defects before the armor, and perhaps after with portable inspection units, is placed into service is critical to their effectiveness[1]. Conventional ultrasonic techniques have been used to both locate and characterize such defects in the monolithic ceramic tiles that make up the "backbone" of these armor panels[2,3]. Furthermore, phased-array ultrasound[4] (PA-UT) has demonstrated significant improvement over these methods[5] as it offers both enhanced sensitivity and improved throughput[67].

PA-UT has also demonstrated its performance with regard to the actual implementation of ceramic armor that incorporates these monolithic tiles into a thick, multi-layered ceramic composite structure[8]. In the current and previous work, a layered structure is used in the assembly of composite armor panels. The panels were made up of tessellated hexagonal high-toughness monolithic ceramic tiles, a carbon-based matrix to encase these tiles, an elastomeric layer to distribute and attenuate mechanical stresses transmitted by the ballistic impact, and a glassy layer which provides a monolithic substrate to support the composite armor. These were arranged as shown in the cross-section and topography of Figure 1. To evaluate defect detectability, planar inclusions of a range of sizes (0.5", 1.5" and 2.5" diameters) were intentionally inserted at the two most critical boundaries (i.e., on either side of the elastomeric bonding layer) to simulate a "disbond" at the locations where it would have the

Report Documentation Page

Form Approved
OMB No. 0704-0188

1. REPORT DATE	2. REPORT TYPE	3. DATES COVERED
30 JAN 2011	**Journal Article**	**30-01-2011 to 30-01-2011**

4. TITLE AND SUBTITLE
COMPOSITE CERAMIC ARMOR DEFECT ANALYSIS USING PHASED ARRAY ULTRASOUND

5a. CONTRACT NUMBER
5b. GRANT NUMBER
5c. PROGRAM ELEMENT NUMBER

6. AUTHOR(S)
J. Steckenrider; Thomas Meitzler; Lisa Prokurat-Franks; W. Ellingson

5d. PROJECT NUMBER
5e. TASK NUMBER
5f. WORK UNIT NUMBER

7. PERFORMING ORGANIZATION NAME(S) AND ADDRESS(ES)
U.S. Army TARDEC ,6501 E.11 Mile Rd,Warren,MI,48397-5000

8. PERFORMING ORGANIZATION REPORT NUMBER
#21445

9. SPONSORING/MONITORING AGENCY NAME(S) AND ADDRESS(ES)
U.S. Army TARDEC, 6501 E.11 Mile Rd, Warren, MI, 48397-5000

10. SPONSOR/MONITOR'S ACRONYM(S)
TARDEC

11. SPONSOR/MONITOR'S REPORT NUMBER(S)
#21445

12. DISTRIBUTION/AVAILABILITY STATEMENT
Approved for public release; distribution unlimited

13. SUPPLEMENTARY NOTES

14. ABSTRACT
A series of 16-inch square by 2-inch thick, multi-layered ceramic composite armor specimens, some of which had intentional design defects inserted between the layers, were inspected using a 128 element, 10MHz immersion phased array ultrasound system. To overcome some of the issues associated with the acoustic wave propagation in layered media, two digital signal processing methods (Fast Fourier Transform (FFT) and Wiener filtering) were employed. While previous work has been presented on the significant improvement in defect detection associated with these methods, the authors present a detailed and quantitative statistical analysis of these results. This analysis suggests that these intentional defects were a) not detectable when the defect was in a particular configuration, b) readily detectable in all cases for alternate defect position configurations, and c) clearly identifiable in most cases for those configurations. However, even in the configuration where intentional defects were not detected (owing to inherent design issues in the armor structure), significant variation in interfacial quality was observed and quantified, and these results will also be presented.

15. SUBJECT TERMS

16. SECURITY CLASSIFICATION OF:			17. LIMITATION OF ABSTRACT	18. NUMBER OF PAGES	19a. NAME OF RESPONSIBLE PERSON
a. REPORT	b. ABSTRACT	c. THIS PAGE			
unclassified	**unclassified**	**unclassified**	**Same as Report (SAR)**	**14**	

greatest effect in reducing the ballistic performance of the panel. While the results of the previous effort showed that the use of FFT and Weiner filtering methods significantly improved defect detection, the current work expands upon those results by quantifying the associated detection limits for various inspection configurations.

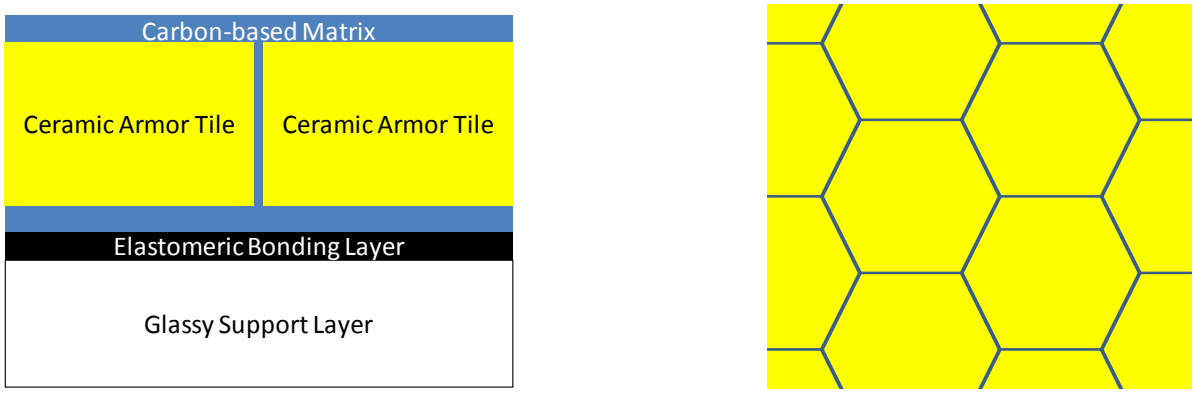

(a) (b)

Figure 1. Schematic diagram of composite layered armor panel: a) cross-section and b) top view.

THEORY

In order to effectively evaluate the ability of Phased-Array Ultrasound (PA-UT) to detect, identify and quantify defects and their severity in composite ceramic armor, it is necessary to evaluate the Signal-to-Noise Ratio (SNR) of the inspection methodology. To do this requires that the noise level of the defect-free inspection be quantified. Since the "data" resulting from a PA-UT inspection is usually an image, it is often necessary to do some type of image processing for best results. In image processing, the SNR is defined as the ratio of the signal mean (in this case, the average pixel intensity in the region known or presumed to be defective) to the standard deviation of the background[9] (the non-defective region of the image), as

$$SNR = \frac{\mu_{sig}}{\sigma_{bg}} \tag{1}$$

However, this assumes that the mean of the background is zero. In situations where this is not the case (i.e., where a low-level response is expected in the background of the image), a more accurate definition would be

$$SNR = \frac{\left(\mu_{sig} - \mu_{bg}\right)}{\sigma_{bg}} \tag{2}$$

As a result, the SNR is simply a measure of how many standard deviations a particular pixel or group of pixels is from the mean of the remainder of the image. This presents two difficulties for PA-UT relative to composite armor inspection. First, this definition of SNR assumes that the pixels of the image (in this case an ultrasonic c-scan image) are normally distributed. While this assumption is valid for shot-noise limited systems (as is the case for ideal optical images)[10], it is not valid for PA-UT images, as will be shown below. Second, the significance of the SNR value is dependent upon the fraction of the total image occupied by the signal pixel(s). For instance, in a 1024 x 1024 image, a single pixel must attain a SNR greater than 4.76 in order to be considered statistically meaningful (i.e., in order to be definitively distinguished from the normal background variation), as this would represent a confidence of roughly 99.9999% (i.e., 1 part in 1024^2), but a 10 x 10 (100 pixel) region within that

image would only need an average SNR of greater than 3.73 in order to be considered statistically meaningful, as this would now represent a confidence interval of only 99.99% (i.e., 100 parts in 1024^2). Thus, it is actually the relationship between the area of the defect and the distribution of pixel intensities in that image that is of greatest interest in determining the detectability of a particular defect. In any case where the confidence interval for the mean intensity of a nominally defective region of the image exceeds the fraction of the image not occupied by the nominally defective region, that region is determined to indeed be defective, as it could not have attained the intensity value it has within the distribution of intensities due to regular fluctuations in the background.

To address the first concern, the distributions of pixel intensities were measured for a number of different composite ceramic armor panels using c-scan data and it was found that these data were indeed not normally distributed. Figure 2a shows a c-scan of panel B3, a defect-free panel used for establishing baseline parameters for the PA-UT methodology, and Figure 2b shows a histogram of the pixel values for the central bright rectangular region of that c-scan. (Note that, for this initial multi-facility study, all panels were sealed with a composite wrap to maintain the integrity of the panel as it was shipped between facilities, and that to insure the integrity of the seal this wrap overlapped the edges of the panel, as shown by the dark frame around the edges of Figure 2a. Thus, the panel surface was uniform only in the central bright region, so only this region was used for quantitative analyses.) Although the Normal Distribution fit in Figure 2b is somewhat close, the χ^2 fit (for which the probability distribution is equally well known as

$$f(x,k) = \frac{1}{2^{(k/2)}\left(k/2-1\right)!} x^{(k/2-1)} e^{-\frac{x}{2}} \tag{3}$$

where x is the pixel intensity value and k is the degrees of freedom) is clearly superior, and would be expected to provide a much more accurate assessment of the confidence interval for each pixel intensity value in the image. A χ^2 fit was used for each panel in order to determine the probability for each pixel intensity. Any pixels that exceeded this probability determined if and where any defects were present. However, because of the significant variation present in this feasibility study (panels were made in batches of four, with sometimes significant variation between batches, were wrapped individually, with significant variation in wrap between panels, and were inspected intermittently over a period of several months through the round-robin protocol established) it was not reasonable or feasible to establish a single baseline intensity distribution for all panels (as would be used in a conventional manufacturing process). Therefore, the intensity distribution for each c-scan was measured and the χ^2 probability density function was individually fit for each panel.

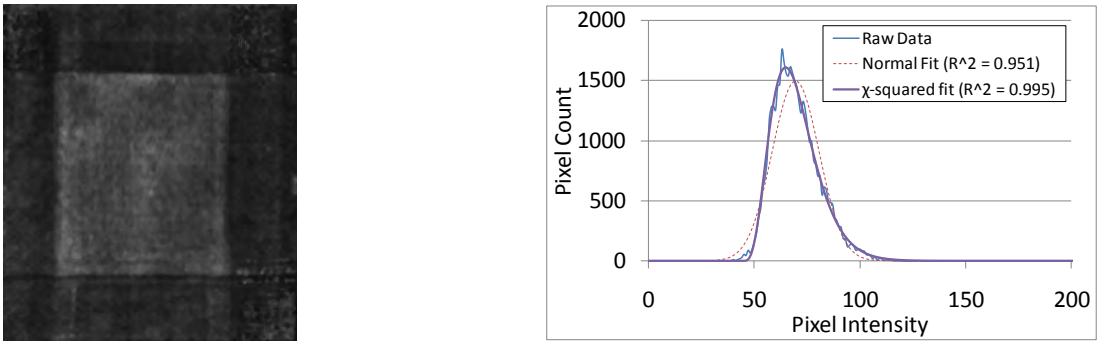

(a) (b)

Figure 2. Example of determination of statistical parameters: a) C-scan image and b) Histogram of intensity values showing Normal and χ^2 distribution fits taken from the central bright rectangular region for panel B3, a defect-free ceramic armor panel.

To address the second concern (establishing the significance of a particular SNR as a function of defect size), intensity values were directly translated into confidence intervals. This yielded a non-linear intensity distribution that was directly correlated to the statistical likelihood that the intensity value would have occurred spontaneously without the presence of a defect. Details of this approach are provided in the Table 1. Example Log LUT values for panel B3

Input Intensity	Cumulative Probability	Log Output Intensity
≤ 46	≤ 0.001%	0
47	0.01%	26
48	0.1%	51
51	1%	77
57	10%	102
68	50%	128
85	10%	153
104	1%	179
119	0.1%	204
135	0.01%	230
≥ 148	≤ 0.001%	255

Intensity Distribution section below.

PROCEDURE

Although the locations of the intentional defects were known for the panels examined in this study, the analytical methodology must work autonomously without user intervention. The analysis procedure prescribed below is therefore designed to operate automatically. However, given the nature of this initial feasibility study, there were some additional steps added to the procedure to compensate for variation present here that would not be included in an ultimate in-process implementation.

Spatial Filtering

The first accommodation that must be made for these preliminary study panels relates to the panel overwrap (which would not be present in full-scale manufacturing evaluations). As mentioned above, these ceramic armor panels were encapsulated in a woven composite wrap to maintain panel integrity throughout the evaluation process. Unfortunately, this wrap altered the ultrasonic coupling efficiency at the surface, so that regions between the fabric fibers transmitted less acoustic energy into the panel than the regions along the fibers. Thus, the raw c-scan data was superimposed with this fiber pattern, as shown in Figure 3a. To reduce the impact of this artificial surface pattern, which carries no information about the bulk properties of the armor panel, a 5-pixel diameter median filter was applied to the image, with the result shown in Figure 3b. Although the effects of the composite weave have been virtually eliminated in Figure 3b, all other features (which exhibit a spatial dimension greater than 5mm) have been retained, and thus are available for further investigation.

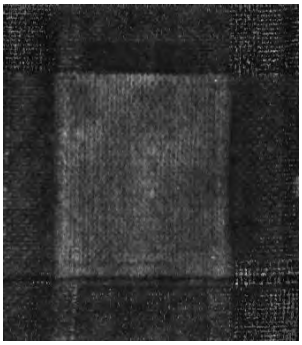

(a)

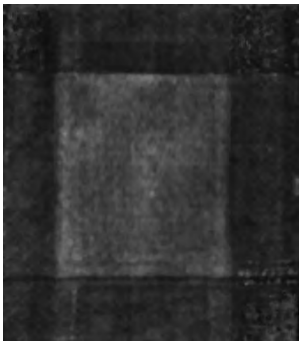

(b)

Figure 3. Example of use of median filtering: a)-PA-UT c-scan of panel B3 as inspected and b) PA-UT c-scan after 5x median filtering.

ROI selection

The second accommodation that must be made for these test panels derives from the fact that only a central portion of the panel, where ballistic impact would ultimately be applied, was constructed according to the actual in-service armor design. The remainder of the panel was built with "filler" material of a lesser quality and cost. Thus, for the feasibility study, a smaller region-of-interest (ROI) in the center of each panel where the ultimate armor materials were used was examined. Because the location of this region varied from panel to panel, the ROI had to be manually selected for each panel. However, the shape of the ROI was known, so only three different selections were used, and these are shown in Figure 4 for inspections from a) the support side (where the 190 mm x 220 mm ROI was limited by the overlapping encapsulating overwrap around the edges), b) the ceramic side (in the cases where a single high-value 102 mm height hexagonal tile was used, for a 7613 mm^2 ROI) and c) the ceramic side (in the cases where three high-value hexagonal tiles were used, for a 25,308 mm^2 ROI).

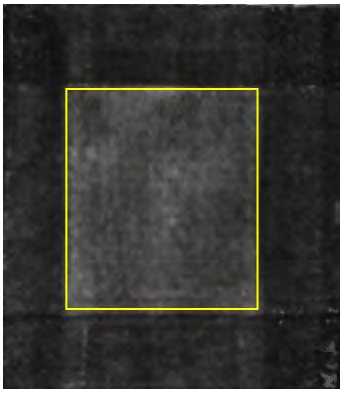

(a)

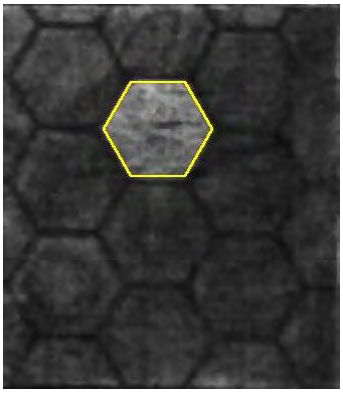

(b)

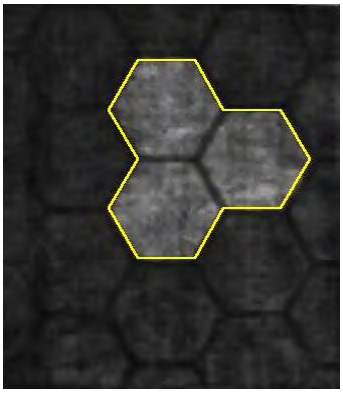

(c)

Figure 4. Selection of Region-of-interest (ROI) definition: a) support-side inspection, b) ceramic-side inspection with a single high-performance tile and c) ceramic-side inspection with three such tiles.

Table 1. Example Log LUT values for panel B3

Input Intensity	Cumulative Probability	Log Output Intensity
≤ 46	≤ 0.001%	0
47	0.01%	26
48	0.1%	51
51	1%	77
57	10%	102
68	50%	128
85	10%	153
104	1%	179
119	0.1%	204
135	0.01%	230
≥ 148	≤ 0.001%	255

Intensity Distribution

A histogram analysis was applied to each panel to determine the distribution of pixel intensities within the ROI. The histogram output was then fit using the distribution of **Error! Reference source not found.** as shown in Figure 2b above to assign a specific probability value to each pixel intensity in the c-scan. A lookup table (LUT) was then created to map the input pixel intensity to its associated cumulative probability. This LUT was a logarithmic one in which input intensities were mapped to orders of magnitude of probability of random occurrence, as shown in Table 1. Here, the cumulative probability shown corresponds to the area of tail of the distribution beyond the pixel value given (i.e., the values peak at 50% for the median pixel value and decrease toward 0% on either side of the median). The limits of the log scale were chosen so that an output intensity of 0 represented the single-pixel limit on the low-amplitude end of the distribution (i.e., the point where the tail of the distribution would represent a total area of less than 0.5 pixels for the ROI used) and 255 represented the single-pixel limit on the high-amplitude end. Because the defects are likely to be small relative to the ROI inspected, this log-scale LUT provides much greater resolution to differentiate background regions that are just randomly bright from statistical outliers that represent actual defects. It should be noted that, because of the nature of the χ^2 distribution, the ability to resolve meaningful variations on the lower end of this distribution is much worse than the ability to resolve them on the upper end. Fortunately, because defects almost always increase the acoustic impedance discontinuity in the specimen, they will increase the reflected acoustic amplitude, and therefore manifest on the upper end of the distribution, where resolution for detecting and differentiating these defects is greatest.

Finally, this LUT is applied to the raw image, yielding a logarithmic mapping of the probability that each pixel actually represents a defect. This is shown below in Figure 5 for panel B3 (again, in which there were no intentional defects present). Figure 5a shows a photograph of the panel, Figure 5b shows the original c-scan of the panel after median filtration, and Figure 5c shows the logarithmic probability plot.

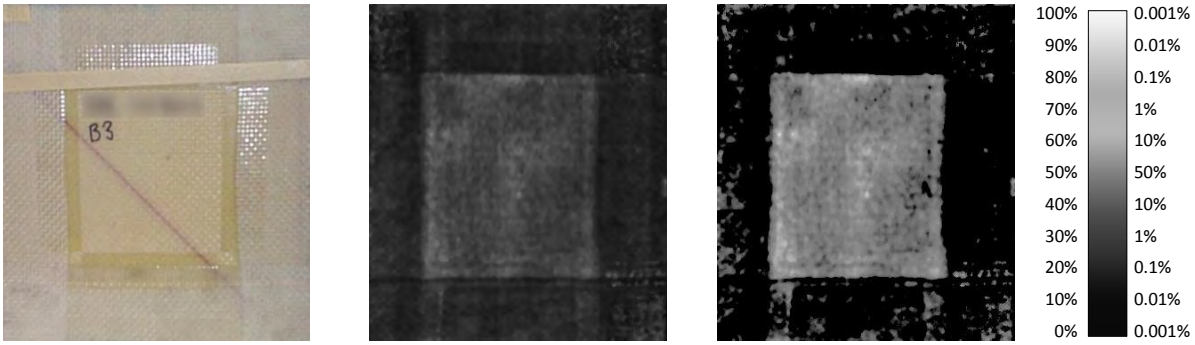

(a) (b) (c)

Figure 5. PA-UT Images of panel B3 showing a) median filtered c-scan, b) photographic image, indicating surface contamination, c) logarithmic map of probability. The scale given corresponds to the probability of random occurrence within the background for c).

Defect Identification

The logarithmic map of probability in Figure 5c shows that even the brightest of the raw c-scan areas are only in the 5% probability range, and therefore are not statistically significant. On the other hand, while the log map shows that there are no regions in which the c-scan amplitude (i.e., pixel intensity) is higher than the background with any statistical significance, it does clearly show that there is a single region on the right-hand side of the ROI in which the probability is zero, indicating a statistically significant difference (i.e., a defect) is present. Although, as stated above, the lower tail of the distribution has a significantly reduced resolution, the size of this area warrants investigation, and is seen in Figure 2b as the slight deviation above the χ^2 fit just below pixel values of 50. However, further analysis of Figure 5b shows that this reduction was likely the product of operator-induced damage in that region, as the "defect" region clearly reflects writing (the name of one of the inspection engineers ("Dick") appears above a series of numbers), where someone appears to have either written on one of the panel layers or used the panel as a writing surface beneath some other medium.

In general, in order to determine whether any portion of a particular c-scan differed from ordinary background variation in a statistically significant way, two methods were used. First, each log mapped image was examined to see if any single pixel value was either 0 or 255. Since the original c-scan had already been subjected to a median filter, any single pixel exceeding the threshold for statistical significance (either high or low) was deemed to represent a defect. Second, the brightest and darkest (i.e., highest and lowest probability) 0.5" diameter regions (a 137-pixel area, due to image pixelization) within the ROI were averaged, and if the tail of the χ^2 distribution beyond this average probability represented a smaller area than the 137 pixels measured then this region was also deemed to represent a defect. However, in cases where an intentional defect larger than 0.5" diameter was present, this larger region size was used to determine the detectability of that known defect.

RESULTS

Given the designed character of the central elastomeric layer to absorb mechanical vibrations, inspection of the panels was performed from both sides – the impact or ceramic side (where the armor tiles were located closer to the surface) and the glassy or support side. Because each of these required a different inspection methodology, they also require unique analysis approaches as well, and therefore are presented separately herein.

Support-side Inspection

Figure 6 and Figure 7 show the median filtered c-scans and log probability maps, respectively, for the J-series of panels. In this series, a 0.5"-diameter inclusion was located between the support and elastomer layers during manufacturing. This inclusion is located directly beneath a single high-value

ceramic tile (albeit on the opposite side of the panel), and is roughly in the center of the ROI for panels J1, J2, J5 and J6, and near the top of the ROI for panels J3 and J4. Knowing its position, the defect can be identified in all six panels, as indicated by the arrow in Figure 6. Furthermore, all defects demonstrated a SNR greater than 1:1, as tabulated in Table 2. However, a more thorough statistical analysis indicates that the only panels in which the defect response differs from the background by a statistically significant amount are panels J1 and J3, as shown in Figure 7. In other words, although the defects show a low probability of random occurrence in all panels (as indicated by a SNR > 1), the predicted area of the tail of the distribution equal to or greater than the average pixel intensity for the defect region (the "Differentiated Area" in the table) is smaller than the area of the actual defect for only these two panels (indicating that, for these c-scans, there are more pixels in the tail of the distribution than would be predicted by the random variation of the background). This means that, if the location of the defect had not been known, it would still have been possible to assign absolute certainty to the presence of defects only in panels J1 and J3.

Figure 8 shows the log probability maps for the N-series of panels. In this series, a 38mm (1.5") -diameter inclusion was located between the support and elastomer layers during manufacturing. This inclusion is located directly beneath the intersection of three hexagonal ceramic tiles (again on the opposite side of the panel), and is located on the left of the ROI for panels N1 and N2, and on the right of the ROI for panels N3 – N6. Note that the outline of the hexagonal tiles in N4 – N6 was the result of surface contamination, which altered the ultrasonic coupling efficiency (i.e., an ink outline of the underlying tiles applied by one of the other inspection facilities) and is not the result of acoustic interaction with these tiles. Again, the SNR for each tile was greater than 1:1, as shown in Table 3. However, in this case, because the area of the defect was larger than in the J-series panels, the defects in all six panels differ from the background by a statistically significant amount. In other words, the maximum area meeting or exceeding the average defect intensity, as predicted from the random variation of the background, is smaller than the actual defect size in all panels. This is also demonstrated in the histogram analysis of Figure 9, where the background variation is well aligned with the χ^2 fit, but the defect manifests a significant deviation from that fit at pixel values centered around 152 (the defect's mean intensity) as encircled by the ellipse in the figure.

Table 2. Defect characteristics for the J-series panels. Defect area = 137 pixels. Shaded defects were definitively, statistically significantly different from the background. SNR was calculated using (2).

Panel #	χ^2 Fit R^2 value	Defect Mean	Confidence Interval	Differentiated Area (pixels)	Defect SNR
J1	0.994	135.6	99.87%	56	4.01
J2	0.993	71.1	89.01%	4595	1.14
J3	0.994	136.7	99.92%	34	4.04
J4	0.991	142.0	92.95%	2945	1.59
J5	0.992	159.2	98.13%	780	2.69
J6	0.992	89.8	96.86%	1312	2.44

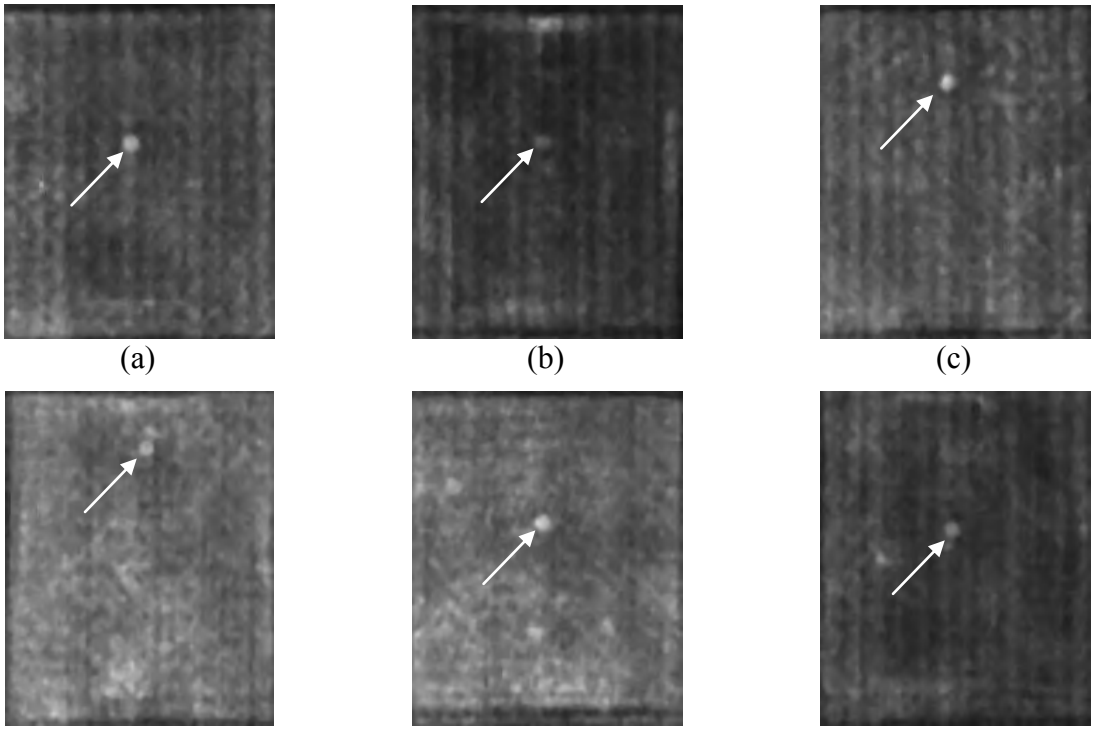

Figure 6. Median filtered support-side inspection c-scan data for panels J1 – J6 (a – f). The intentional defect shown was a 13mm (0.5") diameter inclusion between the support and elastomeric layers, and only the ROI is shown.

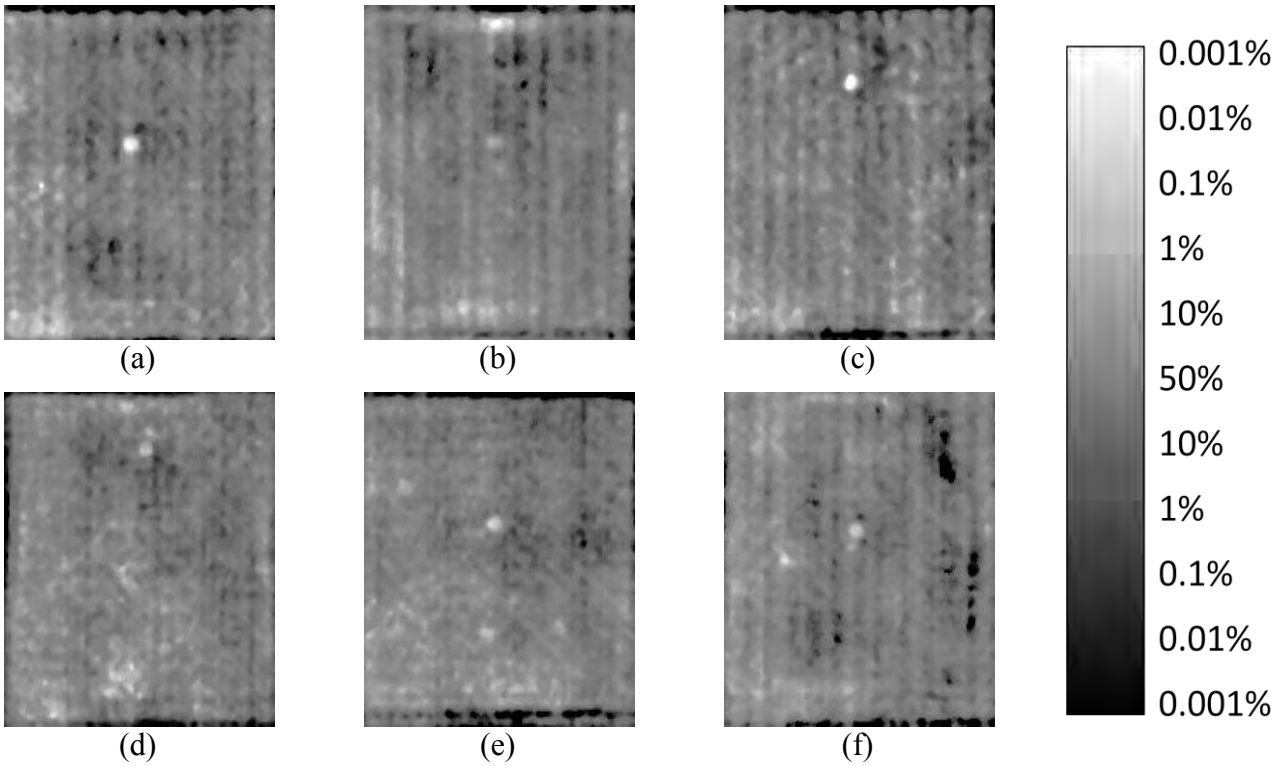

Figure 7. Log probability maps of data from Figure 6 for panels J1 – J6 (a – f). The scale shown references the area of the tail of the distribution beyond that gray-level.

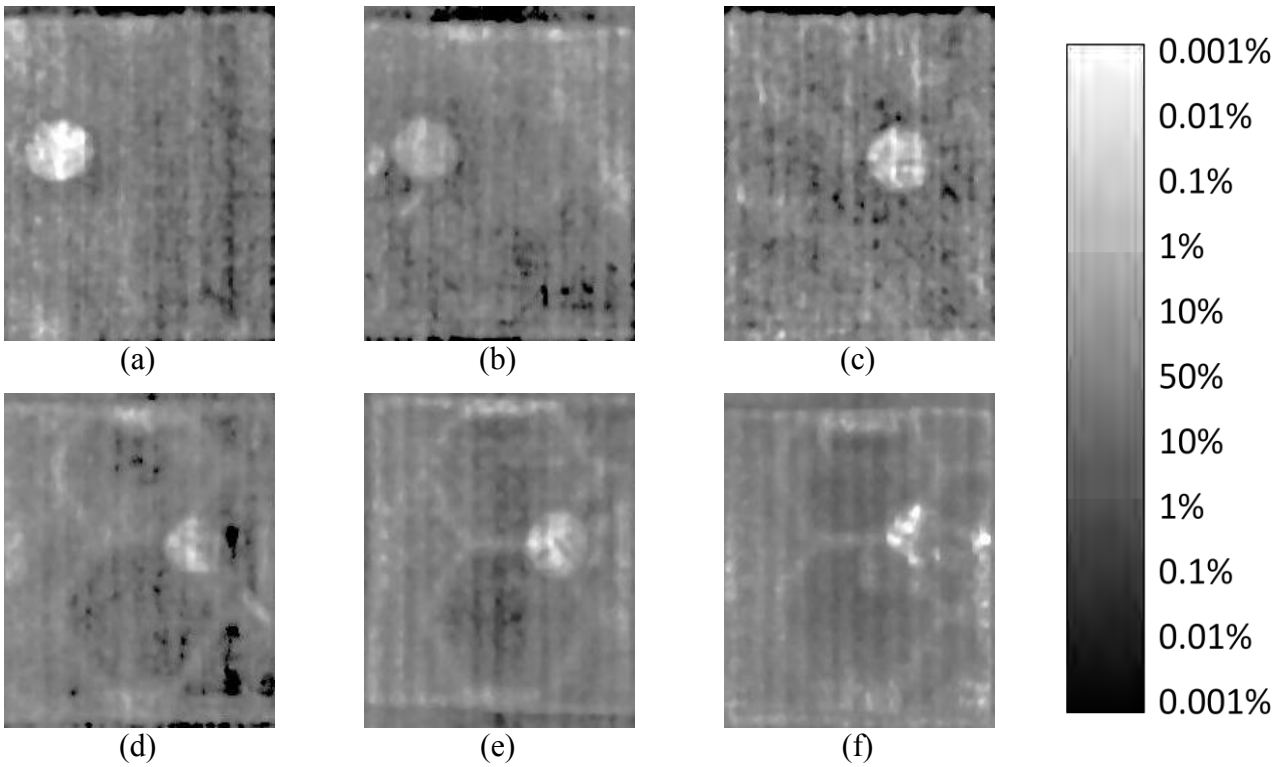

Figure 8. Log probability maps of data for panels N1 – N6 (a – f). The scale shown references the area of the tail of the distribution beyond that gray-level.

Table 3. Defect characteristics for the N-series panels. Defect area: 1134 pixels. Shaded defects were definitively, statistically significantly different from the background. SNR was calculated using (2).

Panel #	χ^2 Fit R^2 value	Defect Mean	Confidence Interval	Differentiated Area (pixels)	Defect SNR
N1	0.994	152.2	99.99%	5	4.96
N2	0.986	167.0	97.70%	961	2.47
N3	0.993	112.4	99.79%	86	4.03
N4	0.985	107.7	97.80%	922	3.09
N5	0.990	129.4	99.32%	285	3.59
N6	0.968	107.4	97.90%	877	2.19

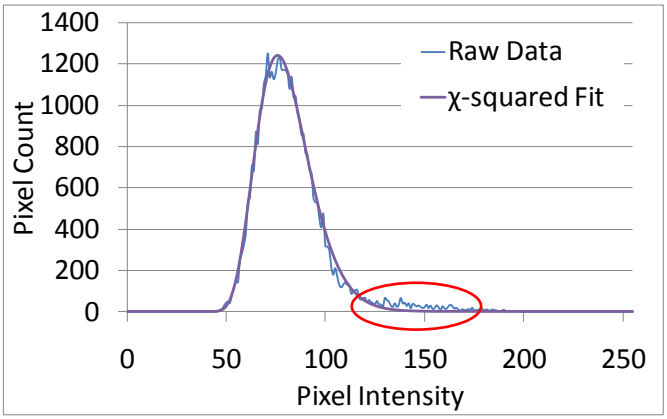

Figure 9. Histogram plot for panel N1, showing both the raw histogram and the χ^2 fit.

Impact or Ceramic-side Inspection

The intentional defects were not visible in the ceramic-side inspections due to the already large mismatch of acoustic impedance between the ceramic layers and the elastomer, hence the lack of a distinct circular region in the centers of Figure 10 and Figure 11. However, these figures do show a significant variation in acoustic amplitude detected (i.e., pixel intensity) so it would seem worthwhile to evaluate the highest and lowest intensity regions in each of these images. Thus, the data presented in Table 4 refers to the highest and lowest 0.5" (13 mm) diameter regions within the ROI of each.

As shown in Table 4, some kind of statistically significant defect was found in all of the D-series panels except D3. The high-intensity defects (shown as shaded rows in the table) showed a definitive statistically significant increase from the background (i.e., increased acoustic impedance mismatch) while low-intensity defects (shown as bold rows in the table) showed a definitive statistically significant decrease from the background (i.e., decreased acoustic impedance mismatch). However, because the slope of the χ^2 distribution is much steeper on the low-intensity side, the ability to resolve small differences in acoustic amplitude in this region is very limited, so the relative significance of this kind of defect may be artificially amplified as a result. Furthermore, a decrease in acoustic mismatch would be more likely to enhance armor performance (as it represents a greater cohesion between the layers), and so these "defects" may not be critical at all. Thus, the areas of greatest importance would be represented by the shaded rows.

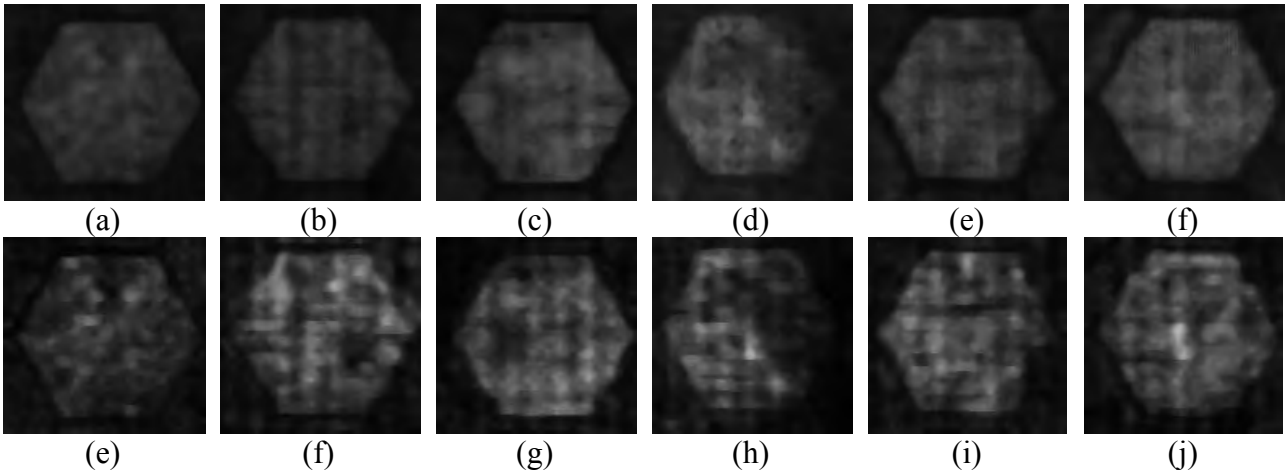

Figure 10. Ceramic-side inspection c-scan data for panels D1 – D6 showing median filtered c-scans derived from Weiner filtering (a – f) and Fourier filtering (e – j) of the a-scans, showing ROI only.

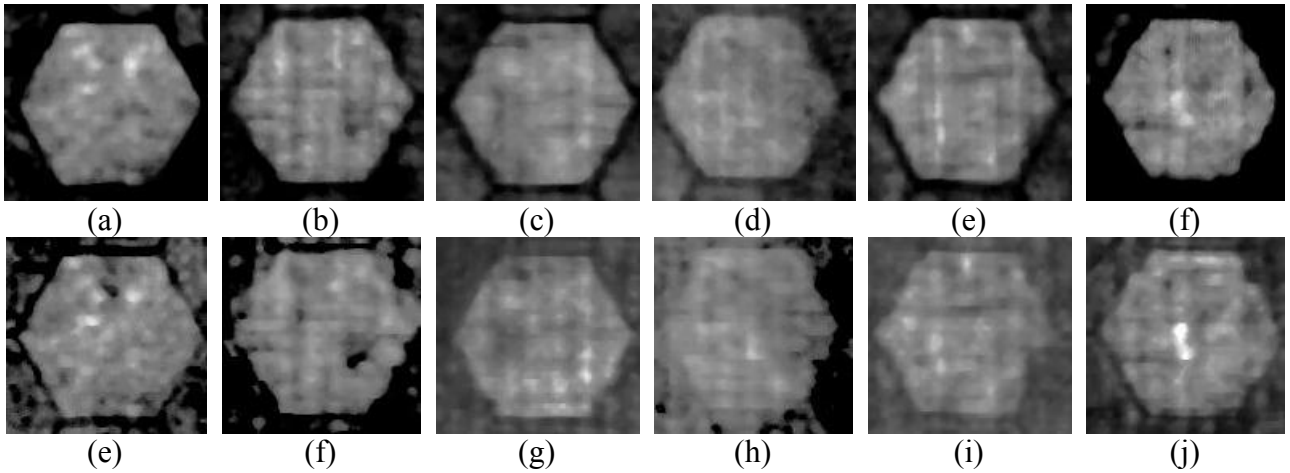

Figure 11. Log probability maps of data from Figure 10 for panels D1 – D6 again derived from Weiner filtered (a – f) and Fourier filtered (e – j) c-scans. Note that only the ROI is shown here.

Table 4. Defect (identified as the 137 pixel areas with the highest and lowest average intensities) characteristics for the D-series panels using both Weiner (Wnr) and Fourier (FFT) filtration of the original PA-UT a-scan data. Shaded rows indicate an increased acoustic impedance mismatch, while bold rows indicate a decreased acoustic impedance mismatch. SNR was calculated using (2).

Panel #	χ^2 Fit R^2 value	Defect Mean	Conf. Interval	Diff. Area	Peak SNR	Valley Mean	Conf. Interval	Diff. Area	Valley SNR
D1-Wnr	0.982	66.0	99.62%	29	2.98	27.949	5.343%	407	1.38
D2-Wnr	0.985	54.1	99.40%	46	2.84	26.453	7.963%	606	1.40
D3-Wnr	0.977	78.1	96.18%	291	2.12	36.774	13.801%	1051	1.14
D4-Wnr	**0.945**	**98.4**	**97.41%**	**197**	**2.53**	**27.796**	**1.195%**	**91**	**2.05**
D5-Wnr	0.971	68.3	92.37%	581	1.54	31.796	3.645%	278	1.76
D6-Wnr	0.966	91.5	98.29%	130	2.29	49.453	6.464%	492	1.33
D1-FFT	0.948	76.4	97.79%	168	2.24	26.445	11.038%	840	1.06
D2-FFT	**0.933**	**116.2**	**92.05%**	**605**	**1.85**	**25.27**	**0.157%**	**12**	**1.72**
D3-FFT	0.942	109.4	96.57%	261	1.90	27.555	3.371%	257	1.81
D4-FFT	0.911	112.9	94.84%	393	2.31	16.292	4.073%	310	1.31
D5-FFT	**0.909**	**109.0**	**85.32%**	**1117**	**1.93**	**20.212**	**1.382%**	**105**	**1.92**
D6-FFT	0.951	128.5	99.78%	17	2.79	34.124	5.321%	405	1.46

Table 5. Defect (identified as the 137 pixel areas with the highest and lowest average intensities) characteristics for the G-series panels using both Weiner (Wnr) and Fourier (FFT) filtration of the original PA-UT a-scan data. Shaded rows indicate an increased acoustic impedance mismatch, while bold rows indicate a decreased acoustic impedance mismatch. SNR was calculated using (2).

Panel #	χ^2 Fit R^2 value	Defect Mean	Conf. Interval	Diff. Area	Peak SNR	Valley Mean	Conf. Interval	Diff. Area	Valley SNR
G1-Wnr	0.991	36.7	95.21%	1213	2.20	7.985	2.157%	546	1.68
G2-Wnr	0.986	37.4	94.84%	1305	2.31	11.102	3.536%	895	1.26
G3-Wnr	0.988	37.6	98.14%	471	2.79	8.825	4.401%	1114	1.41
G4-Wnr	0.995	37.8	99.63%	94	3.50	8.912	6.812%	1724	1.22
G5-Wnr	0.939	50.1	93.56%	1629	2.41	7.577	0.605%	153	1.60
G6-Wnr	0.987	53.7	97.94%	521	2.50	10.409	0.550%	139	1.78
G1-FFT	0.981	97.3	95.49%	1141	2.25	29.883	7.963%	2015	1.32
G2-FFT	**0.986**	**106.7**	**97.76%**	**568**	**2.77**	**22.971**	**0.060%**	**15**	**1.71**
G3-FFT	0.986	114.2	99.60%	102	3.17	31.029	2.662%	674	1.63
G4-FFT	0.987	113.7	99.83%	44	3.76	23.526	9.339%	2364	1.09
G5-FFT	0.944	125.6	96.82%	805	2.90	10.839	2.451%	620	1.57
G6-FFT	0.982	115.7	99.34%	166	3.46	11.905	1.142%	289	1.62

The G-series panels also showed statistically significant high-intensity defects in both panels G3 and G4, as given in Conclusion

Phased-array ultrasonic inspection methods have been successfully applied to layered composite ceramic armor structures. We have demonstrated that the distribution of acoustic amplitude comprising the resulting c-scans (aka pixel intensities) follows a χ^2 distribution much more closely than a normal distribution, and so the conventional application of Signal-to-Noise Ratio is not applicable for this data set. Furthermore, owing to the limited nature of this feasibility study, only a portion of each panel was representative of the "normal" construction of the layered armor design, so only a limited region of interest was evaluated for each panel. Thus, a χ^2 distribution was fit to the histogram of pixel intensities for each ROI and used to determine the statistical probability that each pixel or region of pixels could have occurred by random variation of the acoustic amplitude reflected

from the interface of interest. Any region whose area exceeded that of the tail of this distribution beyond that region's average intensity was therefore definitively identified as a defect.

. The G4 defect was severe enough to be seen in both the Weiner and FFT maps, but the G3 defect was only detected using the FFT method. In addition, a single low-intensity defect was detected in panel G2, but only using the FFT method. Finally, there were two more low-intensity defects detected in panels G4 and G5, but these were much smaller than the 137 pixel critical area used for this evaluation, and so when averaged over a larger area these defects were not statistically significant. Of particular note in this data set was the lack of direct correlation between a traditionally measure SNR (which again assumes a normal distribution) and the χ^2 detection confidence. For example, when examining a 137 pixel region of the G-series panels, a SNR (calculated according to conventional method of (2) above) in excess of 2.55 would determine that the region differed from the random background variation by a statistically significant amount, using a normal approximation to the background variation. Such an approximation applied to the FFT results of Conclusion

Phased-array ultrasonic inspection methods have been successfully applied to layered composite ceramic armor structures. We have demonstrated that the distribution of acoustic amplitude comprising the resulting c-scans (aka pixel intensities) follows a χ^2 distribution much more closely than a normal distribution, and so the conventional application of Signal-to-Noise Ratio is not applicable for this data set. Furthermore, owing to the limited nature of this feasibility study, only a portion of each panel was representative of the "normal" construction of the layered armor design, so only a limited region of interest was evaluated for each panel. Thus, a χ^2 distribution was fit to the histogram of pixel intensities for each ROI and used to determine the statistical probability that each pixel or region of pixels could have occurred by random variation of the acoustic amplitude reflected from the interface of interest. Any region whose area exceeded that of the tail of this distribution beyond that region's average intensity was therefore definitively identified as a defect.

would predict that all but panel G1 were defective (i.e., contained a statistically significant high-intensity defect). However, the more detailed χ^2 analysis shows that, although the highest-intensity region in panel G6 showed a SNR of 3.46 while panel G3 showed a SNR of only 3.17, the region in panel G3 was determined to be definitively a defect, while the region of G6 was not, and none of the regions in panels G2 or G5 (both of which also had SNR values above 2.55) were statistically defective either.

CONCLUSION

Phased-array ultrasonic inspection methods have been successfully applied to layered composite ceramic armor structures. We have demonstrated that the distribution of acoustic amplitude comprising the resulting c-scans (aka pixel intensities) follows a χ^2 distribution much more closely than a normal distribution, and so the conventional application of Signal-to-Noise Ratio is not applicable for this data set. Furthermore, owing to the limited nature of this feasibility study, only a portion of each panel was representative of the "normal" construction of the layered armor design, so only a limited region of interest was evaluated for each panel. Thus, a χ^2 distribution was fit to the histogram of pixel intensities for each ROI and used to determine the statistical probability that each pixel or region of pixels could have occurred by random variation of the acoustic amplitude reflected from the interface of interest. Any region whose area exceeded that of the tail of this distribution beyond that region's average intensity was therefore definitively identified as a defect.

Detailed and quantitative statistical analysis of PA-UT data has demonstrated that this method is able to detect known inclusion defects between the support and elastomeric layers. Defects as small as 0.5" (13mm) diameter were detected with an average SNR of 2.65, and 1.5" (38mm) diameter

defects were detected with an average SNR of 3.39. In addition, the system has demonstrated the ability to definitively identify as statistically significant all of the 1.5" and some of the 0.5" inclusions as defects. Furthermore, while inclusions between the ceramic and elastomeric layers were not detected (owing to the already extremely large acoustic impedance mismatch between these layers), variation within that interface was observed, and in several cases, statistically significant "natural" defects were detected.

REFERENCES

[1] J.M. Wells, W.H. Green and N. L. Rupert—""On the Visualization of Impact Damage in Armor Ceramics", *Eng. Sci. and Eng. Proc.*, **22** (3), H.T. Lin and M. Singh, eds, pp. 221-230 (2002).

[2] J. S. Steckenrider, W. A. Ellingson, and J. M. Wheeler "Ultrasonic Techniques for Evaluation of SiC Armor Tile," in *Ceram. Eng. and Sci. Proc.*, **26** (7), pp. 215-222 (2005).

[3] R. Brennan, R. Haber, D. Niesz, and J. McCauley "Non-Destructive Evaluation (NDE) of Ceramic Armor Testing," in *Ceram. Eng. and Sci. Proc.*, **26** (7), pp. 231-238 (2005).

[4] G.P. Singh and J. W. Davies, "Multiple Transducer Ultrasonic Techniques: Phased Arrays" In Nondestructive Testing Handbook, 2nd Ed., **7**, pp. 284-297 (1991).

[5] J. Scott Steckenrider, William A. Ellingson, Rachel Lipanovich, Jeffrey Wheeler, Chris Deemer, "Evaulation of SiC Armor Tile Using Ultrasonic Techniques," *Ceram. Eng. and Sci. Proc.*, **27** (7), (2006).

[6] D. Lines, J. Skramstad, and R. Smith, " Rapid, Low-Cost, Full-Wave Form Mapping and Analysis with Ultrasonic Arrays", in Proc. 16th World Conference on Nondestructive Testing, September , 2004.

[7] J. Poguet and P. Ciorau, " Reproducibility and Reliability of NDT Phased Array Probes", in Proc. 16th World Conference on Nondestructive Testing, September , 2004.

[8] J.S. Steckenrider, W.A. Ellingson, E.R. Koehl and T.J. Meitzler, "Inspecting Composite Ceramic Armor Using Advanced Signalt Processing Together with Phased-Array Ultrasound," in *Ceram. Eng. Sci. Proc.*, **31** [5] 1-12 (2010).

[9] Russ, John C. *The Image Processing Handbook.* Boca Raton, FL: CRC Press, 2007, p. 26.

[10] Schroeder, Daniel J. *Astronomical Optics.* San Diego, CA: Academic Press, 2000, p. 433.